De-embedding of Contact Pads Parasitics in RFMEMS resonators for 5G Applications

Wenjia Yang
Institute of Microelectronics
*Agency of Science, Technology and Research (A*STAR)*
Singapore
yangwj@ime.a-star.edu.sg

Chen Liu
Institute of Microelectronics
*Agency of Science, Technology and Research (A*STAR)*
Singapore
liuc@ime.a-star.edu.sg

Ying Zhang
Institute of Microelectronics
*Agency of Science, Technology and Research (A*STAR)*
Singapore
zhangying@ime.a-star.edu.sg

Bhattacharya Shashwat
Institute of Microelectronics
*Agency of Science, Technology and Research (A*STAR)*
Singapore
bhattachar@ime.a-star.edu.sg

Xinghua Wang
Institute of Microelectronics
*Agency of Science, Technology and Research (A*STAR)*
Singapore
wangxh@ime.a-star.edu.sg

Eugene Yi Zhun Woo
Institute of Microelectronics
*Agency of Science, Technology and Research (A*STAR)*
Singapore
woo_yi_zhun@ime.a-star.edu.sg

Yao Zhu
Institute of Microelectronics
*Agency of Science, Technology and Research (A*STAR)*
Singapore
yangwj@ime.a-star.edu.sg

***Abstract*— To remove the parasitic reactance in wafer-level measurement of MEMS resonators and derive the relationship between the size of the resonator and how parasitic reactance can affect the performance of the resonator, the line-to-line de-embedding method is applied to the measurement results of resonators with the area of approximate 20000 μm^2 and 10000 μm^2. The line-to-line method is found to be efficient in RF measurement, with a small chip area requirement. The parasitic reactance at high frequency mainly consists of resistive and inductive components and helps to reduce the resonance frequency and increase the resonance impedance of the resonator hence reduction in coupling coefficient is observed after de-embedding for all resonators. Moreover, resonators with large device areas tend to be more affected by the parasitic reactance at high working frequency compare to the smaller ones.**

Keywords*— *RF MEMS, de-embedding, Line-to-Line, parasitic reactance, FBAR

I. Introduction

The working frequency of MEMS devices experiences a continuous increment for the past few years. To successfully characterize the device, an accurate measuring method is hence necessary. With a working frequency exceeding 4.5 GHz, which is common in current 5G applications, the parasitic reactance from the contact pad and metal interconnect becomes non-negligible compared to sub-GHz applications, causing errors and faulty characterization in wafer-level measurement. To overcome this issue, de-embedding is necessary for 5G applications [1], and de-embedding structures are implemented to remove the parasitic effects for the device under testing (DUT). Commonly practiced de-embedding methods include the open-short method and the open-short-through method [2-3]. The former employs an open and short structure to remove the parasitic reactance in the contact pad and faces difficulty to remove the metal interconnect parasitic reactance. The latter one requires three de-embedding structures for each device and hence there is a large requirement for the wafer area. In this paper, we employ the line-to-line (L2L) de-embedding method for parasitic reactance removal [4]. The method utilizes a transmission line structure to represent the metal interconnect in the device, and two de-embedding structures can be shared by multiple devices in wafer-level measurement, thereby significantly reducing the chip area needed for de-embedding, when compared with the open-short-through method. We conduct measurements on FBARs with large and small device areas and then implement the L2L de-embedding method on all of them. Based on the derived parasitic reactance, we further construct a parasitic modified Butterworth-Van Dyke (pmBVD) model to validate the accuracy and repeatability of the L2L de-embedding method. By comparing the raw and de-embedding results, we discover that the parasitic effects mainly influence the performance of the resonator at its resonance frequency and have a bigger effect on the device with a larger area compared to the small ones.

II. De-embedding Methods

A. Line-to-Line (L2L) de-embedding method

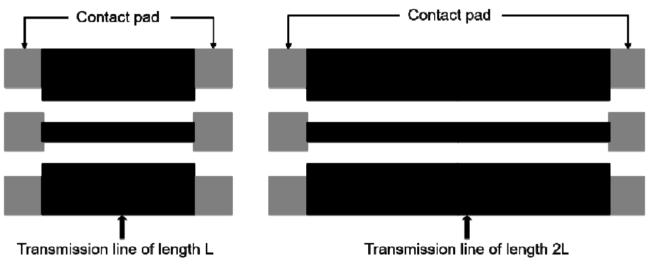

Figure 1. Structures employed for L2L de-embedding

The Line-to-Line method employs a transmission line with different lengths for the contact pads and metal interconnect parasitic extraction. Figure 1 depicts the structure employed by the L2L de-embedding method, a transmission line of 50Ω is placed between two sets of contact pads. The left structure has a transmission line with length L and the right with length 2L.

If both structures are viewed as cascaded two-port networks containing a left pad matrix, transmission line matrix (TLine), and right pad matrix, and assume all matrices are symmetrical and the transmission line is uniform with length, using their ABCD matrix two structures can be then written as [5]:

$$[L] = [pad]\times[TLine]\times[pad]$$

$$[2L] = [pad]\times[TLine]\times[TLine]\times[pad] \qquad (1)$$

Where [L] and [2L] are the measured results of the left and right structures in Figure 1. The pad and TLine matrix can be derived as:

$$[pad] = [[L]\times[2L]^{-1}\times[L]]^{1/2}$$

$$[TLine] = [pad]^{-1}\times[L]\times[pad]^{-1} \qquad (2)$$

For any device with raw measurement results, its de-embedding results can be derived by removing the pad and TLine matrices from it, and hence:

$$[raw] = [pad]\times[TLine]\times[DUT]\times[TLine]\times[pad]$$

$$[DUT] = [TLine]^{-1}\times[pad]^{-1}\times[raw]\times[pad]^{-1}\times[TLine]^{-1} \quad (3)$$

The DUT matrix is transferred back into the scattering parameter (S parameters) to characterize the performance of the device. A full description of the L2L de-embedding method can be found in [5].

B. *Parasitic mBVD (pmBVD) model*

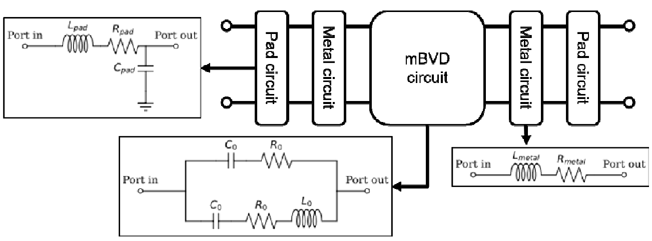

Figure 2. The constructed pmBVD model

To validate the L2L de-embedding method, a pmBVD model is constructed. The circuit model contains two pad circuits and two metal interconnect circuits, which form the parasitic parts, and one mBVD circuit, which represents the DUT actual performance. The pad circuit contains one pair of series-connected inductor and resistor representing the contact impedance, as well as a parallel connected capacitor representing the inter-pad capacitance. The metal interconnect circuit contains a pair of series-connected inductor and resistor. All the circuit elements in the parasitic circuits are extracted from the L2L matrices [pad] and [TLine], and it is assumed that for all devices the parasitic circuits remain constant. The mBVD model can be then extracted from the pmBVD model and used to compare with the L2L de-embedding result to validate the accuracy and efficiency of the de-embedding. All circuit simulation is completed using the Keysight ADS simulator.

III. RESULTS AND DISCUSSION

A. *Fabrication of FBARs with different device areas*

FBAR resonators with the same stack thickness but different device areas are fabricated using Mo/AlN/Mo material stack. Figure 3 illustrates the top and cross-sectional view of the FBARs fabricated in this paper. The top electrode is made of 150 nm Moly, the bottom electrode is made of 100 nm Moly, and the piezoelectric layer is made of a 500 nm thick AlN film. The large devices have an electrode area of 22700 μm^2, and the small devices have an electrode area of 10300 μm^2. The metal interconnect region for the big and small devices, which is pointed out by the black arrow in Figure 3, has a slight difference in length with minimal variation in their parasitic effects. The fabrication process can be referred to in our previous work [6].

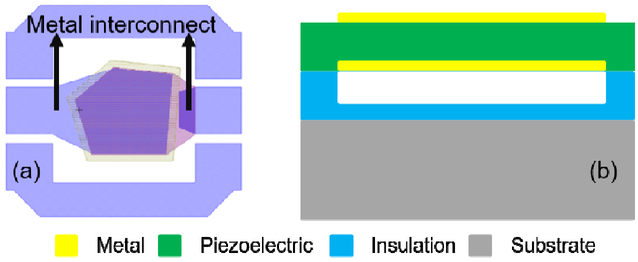

Figure 3. (a) top view and (b) cross-sectional view of the fabricated FBAR in this paper

B. *L2L de-embedding of FBARs with various sizes*

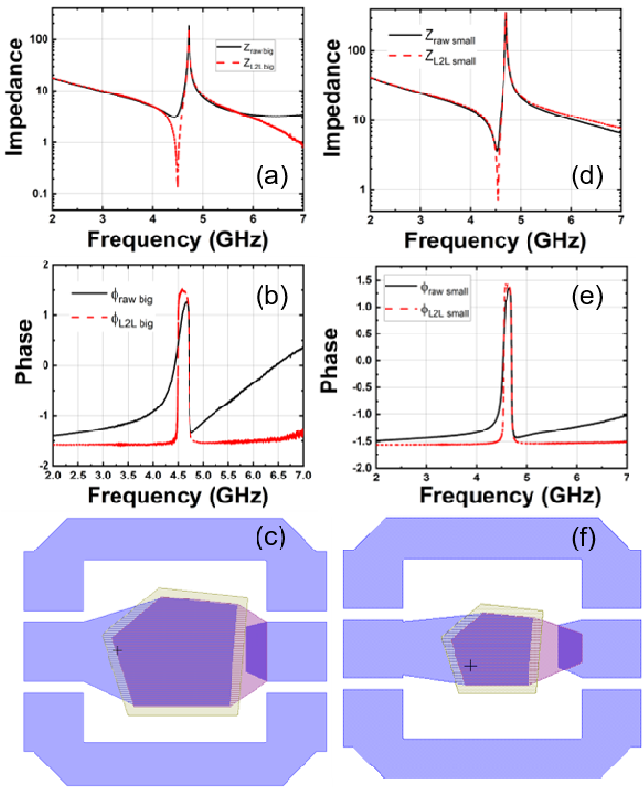

Figure 4. (a) the impedance plot, (b) the phase plot, and (c) the layout of the big FBAR before (black) and after (red) de-embedding, and (d) impedance plot, (e) phase plot, and (f) layout of small FBAR before (black) and after

The L2L de-embedding is carried out on both large and small devices to evaluate how de-embedding can affect the measurement results and to investigate which type of devices tend to be more affected by the same parasitic components. Figure 4 shows the responses of two types of FBARs before and after de-embedding. Regardless of the size of the device, the de-embedding process removes excessive inductance and resistance coming from the metal interconnect and the contact pad, and hence the resonance impedance, Z_s, is reduced. As the inductive parts are removed, the resonance frequency, f_s of the device increases, leading to a smaller coupling coefficient as well. Moreover, devices with a larger area are more affected by the same parasitic reactance when compare to that of the smaller devices, as the changes due to the de-embedding of on left three subfigures in Figure 4 are more obvious than the changes in the right three subfigures. To further validate this trend, we conduct the same de-embedding on 36 big and 36 small FBARs with the stated device area and summarize the results before and after de-embedding.

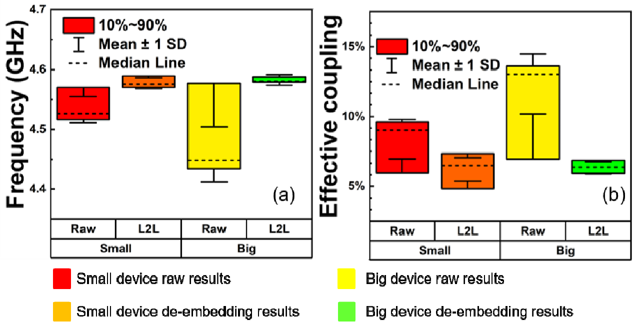

Figure 5. (a) the extracted f_s of 36 big and small devices before and after de-embedding, and (b) the extracted coupling coefficient, k_{eff}^2 of the same devices. The bar indicates the range of the results, dotted line indicates the median of the results

Figure 5 shows the summary of measurement results for 36 devices with big and small sizes. The increment of f_s and reduction of the coupling coefficient, k_{eff}^2 occur for all FBARs, which is in accordance with our previous conclusion. Moreover, the change between yellow and green bars, representing the change due to de-embedding for the big devices, is more obvious and significant than the change between red and orange bars, which is for the small device is also in accordance with our conclusion that large device tends to be more affected by the parasitic effects. Lastly, the green and orange bar is much smaller than the red and yellow bar, indicating after the de-embedding process, the uniformity in device performance and measurement results of both small and large devices improves significantly.

C. Validation of de-embedding with pmBVD model

To further validate the accuracy of the L2L de-embedding method, the pmBVD model is developed to fit the raw measurement results. The mBVD part is then used to compare with the L2L de-embedding result to confirm the accuracy of the de-embedding, for both big and small devices. Figure 6 shows the comparison of the pmBVD model and the raw measurement results, and Figure 7 shows the comparison of the extracted mBVD model and the L2L de-embedding result. Good matchings are observed between the raw data and the pmBVD model, as well as the de-embedding results and the mBVD model, indicating the accuracy of the de-embedding process. Table I shows the extracted parasitic elements from the L2L de-embedding and the ADS fitting results for big and small devices. It shows the results from the L2L de-embedding method agree well with the pmBVD model. The small variation between the metal interconnect components is likely due to the small variation in metal length.

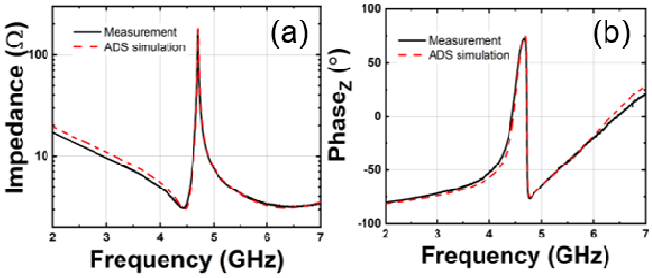

Figure 6. (a) and (b) the impedance and phase plot of the raw measurement result (black) and the pmBVD result (red).

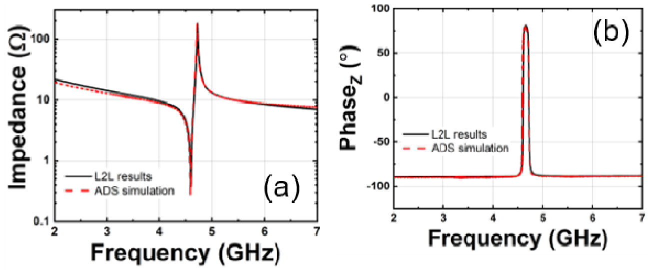

Figure 7. (a) and (b) the impedance and phase plot of the L2L de-embedding result (black) and the extracted mBVD result (red).

From the circuit model, a reduction in resonance impedance and an increment in resonance frequency are also observed. Hence, we conclude that the parasitic components predicted by the L2L de-embedding method are accurate. With two extra structures for de-embedding, the L2L method can be employed for the de-embedding of multiple devices, thereby saving a significant amount of chip area.

TABLE I. Pad (top) and metal interconnect circuit (bottom) for all methods

Pad circuit	***L2L***	***pmBVD (small)***	***pmBVD (big)***
R_p (Ω)	**1.5**	**1.52**	**1.42**
L_p (H)	**2.5e-11**	**2.0e-11**	**2.0e-11**
C_p (F)	**NA**	**2.87e-14**	**2.87e-14**
Metal Interconnection	***L2L***	***pmBVD (small)***	***pmBVD (big)***
R_{metal} (Ω)	**NA**	**0.04**	**0.02**
L_{metal} (H)	**7.8e-11**	**8.7e-11**	**7.8e-11**

IV. CONCLUSION

In this paper, we illustrate the application of the line-to-line de-embedding method to resonators with different device areas. The method can successfully remove the parasitic reactance from the contact pad and the metal interconnect to recover the real performance of the resonators with various device sizes, and the requirement of chip area is minimal. Moreover, by comparing the de-embedding results, we discover that large devices tend to be more affected by the parasitic reactance from the metal interconnect, and by removing them a uniform performance for various devices can be obtained.

ACKNOWLEDGMENT

This work was supported by the Science and Engineering Research Council of A*STAR (Agency for Science, Technology and Research) Singapore, under Grant No. A20G9b0135.

REFERENCES

[1] A. Aktas and M. Ismail, "Pad de-embedding in RF CMOS," in *IEEE Circuits and Devices Magazine*, vol. 17, no. 3, pp. 8-11, May 2001, doi: 10.1109/101.933786.

[2] T. Hirano, K. Okada, J. Hirokawa, and M. Ando, "Accuracy investigation of the de-embedding technique using open and short patterns for on-wafer RF characterization," *2010 Asia-Pacific Microwave Conference*, Yokohama, Japan, 2010, pp. 1436-1439.

[3] M.H. Choo, et al., "A novel cascade-based de-embedding method for on-wafer microwave characterization and automatic measurement," *Proc. IEEE MTT-S Int. Microwave Symposium*, FortWorth, TX, June 6-11, 2004, pp. 1237-1240.

[4] J. Song., et al., "A de-embedding technique for interconnects," *Proc. Electrical Performance of Electronic Packaging*, Cambridge, MA, October 29- 31, 2001, pp. 129-132.

[5] Takayama, N., et al., "A de-embedding method using different length transmission lines for mm-wave CMOS device modeling," *IEICE Transactions on Electronics*, vol. 93, no. 6, pp. 812-819, 2010.

[6] Y. Zhu, et al., "A high coupling coefficient 2.3-GHz AlN resonator for high band LTE filtering application," *IEEE Electron Device Letters*, vol. 37, pp. 1344-1346, 2016, DOI: 10.1109/LED.2016.2602852.